Keratins regulate protein biosynthesis through localization of GLUT1 and -3 upstream of AMP kinase and Raptor

Preethi Vijayaraj,[1,2,4] Cornelia Kröger,[1,2] Ursula Reuter,[1,2] Reinhard Windoffer,[3] Rudolf E. Leube,[3] and Thomas M. Magin[1,2]

[1]Abteilung für Zellbiochemie, Institut für Biochemie und Molekularbiologie and [2]Bonner Forum Biomedizin, Universität Bonn, 53115 Bonn, Germany
[3]Institut für Molekulare und Zelluläre Anatomie, Rheinisch-Westfälische Technische Hochschule Aachen Universität, 52074 Aachen, Germany
[4]Center for Vascular Biology Research, Department of Medicine, Beth Israel Deaconess Medical Center, Harvard Medical School, Boston, MA 02215

Keratin intermediate filament proteins form cytoskeletal scaffolds in epithelia, the disruption of which affects cytoarchitecture, cell growth, survival, and organelle transport. However, owing to redundancy, the global function of keratins has not been defined in full. Using a targeted gene deletion strategy, we generated transgenic mice lacking the entire keratin multiprotein family. In this study, we report that without keratins, embryonic epithelia suffer no cytolysis and maintain apical polarity but display mislocalized desmosomes. All keratin-null embryos die from severe growth retardation at embryonic day 9.5. We find that GLUT1 and -3 are mislocalized from the apical plasma membrane in embryonic epithelia, which subsequently activates the energy sensor adenosine monophosphate kinase (AMPK). Analysis of the mammalian target of rapamycin (mTOR) pathway reveals that AMPK induction activates Raptor, repressing protein biosynthesis through mTORC1's downstream targets S6 kinase and 4E-binding protein 1. Our findings demonstrate a novel keratin function upstream of mTOR signaling via GLUT localization and have implications for pathomechanisms and therapy approaches for keratin disorders and the analysis of other gene families.

Introduction

Embryonic development is a fine-tuned interplay of rapid cell growth and differentiation. It is governed by signaling processes that are coordinated in a spatiotemporal manner through interactions with cytoskeletal and scaffold proteins such as keratins in epithelia. However, the function of keratins in spatiotemporal scaffolding and signaling control is unclear. K7, -8, -18, and -19 represent the first keratins during mouse development and begin to form a primary cytoskeleton at nascent desmosomes in the trophectoderm (Jackson et al., 1980). From then on, these keratins are present in all embryonic and extraembryonic epithelia. Owing to their redundancy, it has not been possible to assign and discriminate their mechanical and signaling functions during embryo development and in tissue homeostasis (Hesse et al., 2000; Tamai et al., 2000; Jaquemar et al., 2003). The former is highlighted by previous gene knockout (KO) studies, which have arrived at contradictory results (Baribault et al., 1993; Magin et al., 1998; Hesse et al., 2000; Tamai et al., 2000; Jaquemar et al., 2003). Deletion of K8 caused an embryonic lethal phenotype at embryonic day (E) 12.5, which is associated with placental malfunctions caused by maternal TNF-induced apoptosis (Baribault et al., 1993; Jaquemar et al., 2003). Deletion of K18 permitted normal development because of the presence of K19, illustrating functional redundancy, at least for these two keratins (Magin et al., 1998). The combined deletion of K18/K19 and of K8/K19, which eliminated redundancy, caused fragility of giant trophoblast cells followed by extensive hemorrhages, which led to death at ∼E10 (Hesse et al., 2000; Tamai et al., 2000). This was

P. Vijayaraj and C. Kröger contributed equally to this paper.

Correspondence to Thomas M. Magin: t.magin@uni-bonn.de

Abbreviations used in this paper: 4E-BP1, 4E-binding protein 1; AMPK, AMP kinase; E-cadherin, epithelial cadherin; ES, embryonic stem; KO, knockout; MICER, Mutagenic Insertion and Chromosome Engineering Resource; mTOR, mammalian target of rapamycin; S6K, S6 kinase; WT, wild type.

The Rockefeller University Press $30.00
J. Cell Biol. Vol. 187 No. 2 175–184
www.jcb.org/cgi/doi/10.1083/jcb.200906094

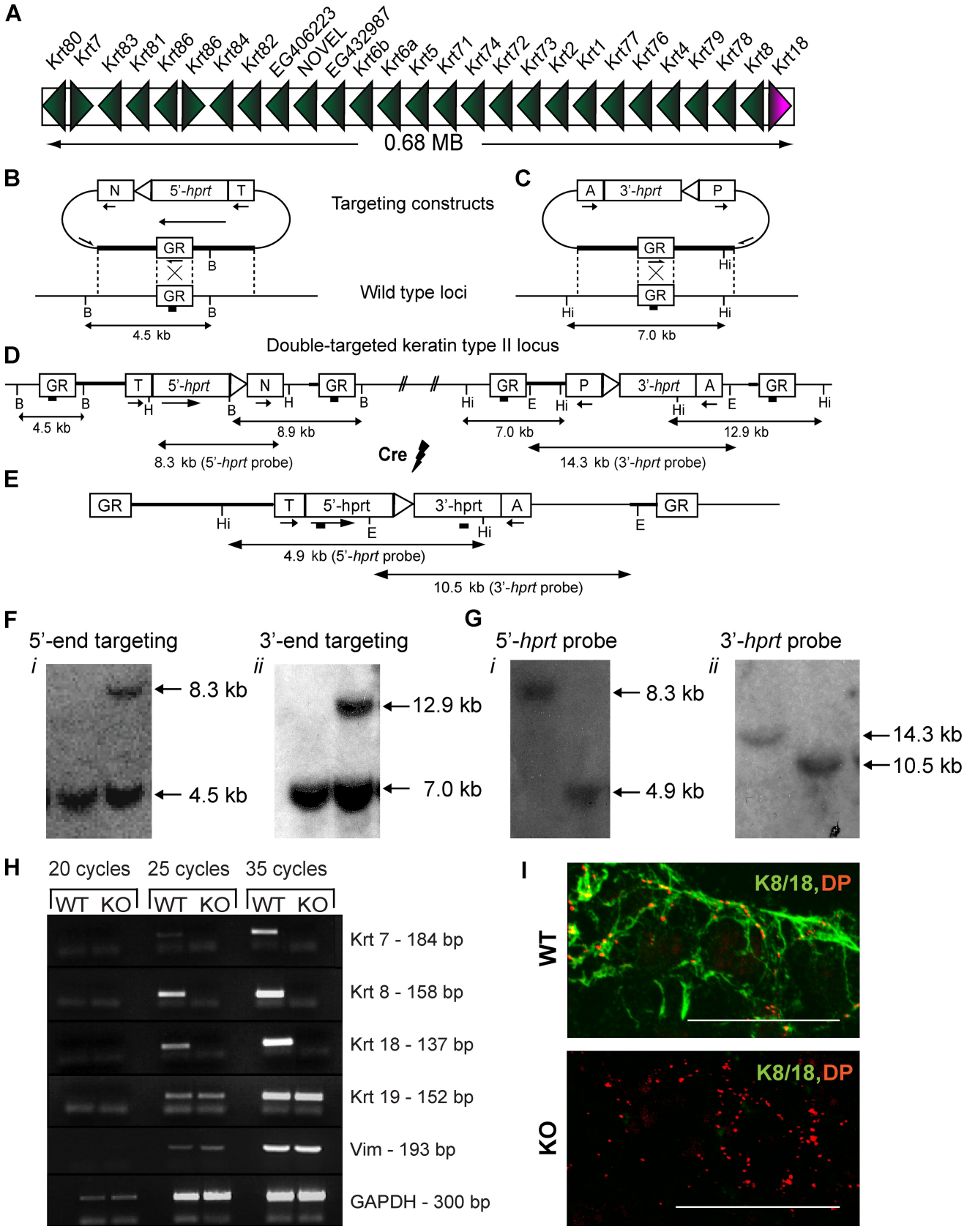

Figure 1. **Constitutive deletion of *Ktyll*$^{-/-}$ keratin gene locus.** (A) Schematic representation of the keratin type II cluster. Green arrowheads identify type II keratin genes oriented in the direction of the tip. The pink arrowhead identifies the only type I keratin (*Krt18*) at the end of type II cluster. (B) 5′-targeting vector (MHPN117k13; Adams et al., 2004). (C) 3′-targeting vector (MHPP322c09; Adams et al., 2004). Gaps [GR] are introduced into the region of homology before targeting. (D) During homologous recombination, the gap is repaired. PCR primers to identify homologous recombinants spanned the gap

interpreted to indicate a primary mechanical function of keratins, which is analogous to that seen in skin epidermis (Fuchs and Cleveland, 1998; Hesse et al., 2000; Tamai et al., 2000; Kim and Coulombe, 2007; Magin et al., 2007).

To systematically analyze keratin functions during embryo development, we exploited the genomic organization of keratin genes. The mouse type I and II keratin families are clustered on two contigs, which are located on chromosomes 11 and 15, respectively (Hesse et al., 2001, 2004; Schweizer et al., 2006). In this study, we describe mice lacking the type II gene cluster. Given that the assembly of keratin filaments from heterodimers requires one member from each family and that keratins are rapidly degraded in the absence of a dimerization partner, mice lacking the type II gene cluster should be devoid of the entire keratin multiprotein family.

Results and discussion

To test current hypotheses on keratin function in mouse development, we used the Cre-loxP system (Ramírez-Solis et al., 1995) to flox the type II keratin gene cluster spanning 0.68 Mb of the genome in mouse embryonic stem (ES) cells (Fig. 1 A; Hesse et al., 2004). Targeting constructs from the Mutagenic Insertion and Chromosome Engineering Resource (MICER; Adams et al., 2004) were engineered with gaps to aid in insertional targeting (Fig. 1, B and C; and Fig. S1 A). Southern blotting confirmed correct targeting at a frequency of 8% (Fig. 1, F and G; and Fig. S1 A). Empty 3′ and 5′ *hprt* vectors labeled for in situ hybridization against spread chromosomes from double-targeted ES cell clones identified double-targeted clones in cis (Fig. S1 B). The floxed gene cluster contained all type II keratins and the type I keratin Krt18, which with K8 forms the first keratin pair during embryonic development (Fig. 1 A; Lu et al., 2005), but no other known genes, including microRNA genes.

Cre-mediated deletion of the keratin type II cluster (Fig. 1, D and E) did not affect ES cell pluripotency, and mice with a constitutive deletion of the keratin type II cluster ($KtyII^{-/-}$) were generated. Deletion of all 27 keratin genes was confirmed by RT-PCR and immunofluorescence microscopy (Fig. 1, H and I; and Fig. 2). Consistent with the proteolytic sensitivity of type I keratins in the absence of their type II keratin binding partners, the sole embryonic type I keratin K19 was expressed at the mRNA but not at the protein level (Fig. 1 H and Fig. S1 D; Magin et al., 2007). Therefore, our mice lack all 54 mammalian keratins (Fig. 1 H). The type III intermediate filament protein vimentin, which is frequently up-regulated during epithelial-mesenchymal transition after loss of keratin expression (Thiery, 2002; Yang and Weinberg, 2008), was not up-regulated at the transcript or protein level, indicating that deletion of the $KtyII^{-/-}$ cluster did not grossly perturb epithelial cell morphology or function (Fig. S2). In support, the expression of the constitutive chaperone Hsc70, which can bind keratins (Liao et al., 1997; Betz et al., 2006), was unaltered. The stress-inducible Hsp70 was not detectable (see Fig. 4 A). Furthermore, activity of MAPK, as examined by Western blotting of candidate target proteins, appeared largely unchanged (see Fig. 4 C).

All $KtyII^{-/-}$ mice died at ∼E9.5 (Fig. S1 E). Because keratins maintain tissue integrity by interacting with desmosomes to provide intercellular adhesion, we investigated the gross appearance and histology of E9.5 embryos. Unlike previous single or double keratin KO mice, which suffered from cytolysis and hemorrhages (Baribault et al., 1993; Hesse et al., 2000; Tamai et al., 2000), $KtyII^{-/-}$ embryos had intact embryonic and extraembryonic epithelia (Fig. 3, A–F). These findings suggest that keratins have no essential mechanical function until this stage of mouse development and that the phenotype of previous keratin KOs may result from dominant-negative effects. Yet, the desmosomes in $KtyII^{-/-}$ embryos were smaller and partially mislocalized (Figs. 1 I and 2, A and B), which is consistent with the involvement of keratins in desmosome assembly (Godsel et al., 2005). During epidermal differentiation, desmoplakin was reported to regulate microtubule organization through ninein (Lechler and Fuchs, 2005). Staining for ninein revealed a prominent localization along the plasma membrane of yolk sac tissue (not depicted) and at centrosomes in embryonic epithelia (Fig. 2 C). Ninein-positive centrosomes retained their apical position in $KtyII^{-/-}$ embryos (Fig. 2 C′), which is in agreement with unaltered γ-tubulin staining (not depicted). This is in contrast to a previous study (Ameen et al., 2001), indicating other and possibly compensatory mechanisms involved in centrosome positioning. The localization of the adherens junction protein epithelial cadherin (E-cadherin) and the tight junction–associated proteins ZO-1 and occludin were highly similar in both genotypes of embryos, indicating that actin-associated adhesion complexes and the actin cytoskeleton (not depicted) maintain epithelial integrity and polarity (Fig. 2, D–F).

$KtyII^{-/-}$ embryos exhibited a striking growth retardation, which started at ∼E8.5 and was fully apparent 1 d later (Fig. 3, G–J). Before the onset of placenta formation at E9.5, the embryo is fully dependent on the yolk sac for nutrient supply. The mammalian target of rapamycin (mTOR) C1 complex regulates protein synthesis by integrating growth factor signals and nutrients. Stimulation of the mTORC1 complex up-regulates protein synthesis by phosphorylation of its downstream targets ribosomal protein S6 kinase (S6K) and eukaryotic initiation factor 4E-binding protein 1 (4E-BP1; Wullschleger et al., 2006). We hypothesized that the embryonic mortality was caused by defective energy metabolism in the yolk sac.

and the proximal vector sequences (Table S1). (E) Cre-mediated recombination between *loxP* sites in cis leading to deletion of the keratin cluster. Southern probes are indicated as bold bars in B–E. (F) Southern blot analysis of ES cell clones targeted at the 5′ (i) and the 3′ end (ii) with a probe that distinguishes BsrGI (B) and HincII (Hi) fragments in the WT and targeted allele, respectively. (G) Southern blot analysis of ES cells after Cre-mediated recombination using unique probes spanning the 5′ and 3′ *hprt*. Probes distinguish double-targeted 8.3-kb and recombined 4.9-kb HinDIII (H) fragments using the 5′ *hprt* probe (i) and double-targeted 14.3-kb and recombined 10.5-kb EcoRI (E) fragments using the 3′ *hprt* probe (ii). (H) mRNA expression of keratins and vimentin (Vim) in E9.5 WT and mutant embryos. Glyceraldehyde 3-phosphate dehydrogenase (GAPDH) was used as a normalization control. (I) Immunofluorescence of K8/ K18 desmoplakin (DP) on sections of E9.5 WT and KO embryos. Bars, 10 µm.

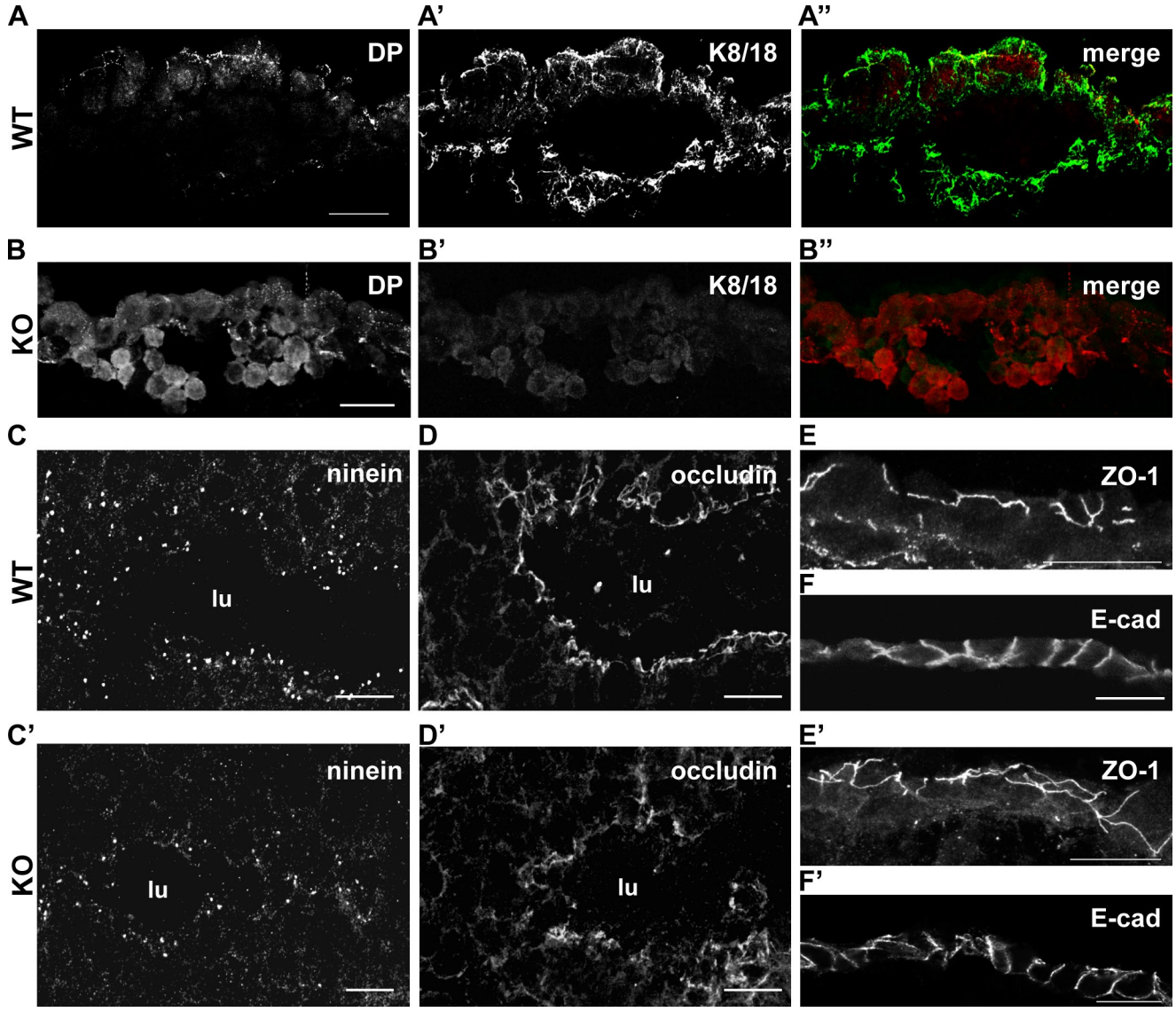

Figure 2. ***Ktyll*$^{-/-}$ embryos show reduced and mislocalized desmoplakin, whereas adherens junctions and cell polarity are unaltered.** (A and B) Double immunolabeling of keratin and desmoplakin (DP) on yolk sac indicates altered distribution and size of desmosomes in the presence (A) and absence (B) of keratins in yolk sac tissue. (C) Ninein part of the microtubule-organizing center complex at the centrosomes is located apically in WT (C) and KO embryonic intestine (C′). (D) Note the apical localization of occludin, a transmembrane protein of tight junctions. (E) Antibody staining of the tight junction marker ZO-1 in the yolk sac revealed no changes in WT (E) compared with *Ktyll*$^{-/-}$ (E′) E9.5 embryos. (D and E) ZO-1 and occludin are located at the apical plasma membrane of the yolk sac and the intestine, respectively, indicating normal cell polarity. (F) Intact adherens junctions in mutants (F′) and their WT littermates (F), as demonstrated by staining for E-cadherin (E-cad) in yolk sac tissues of E9.5 embryos. lu, lumen. Bars: (A–B″ and E–F′) 10 µm; (C–D′) 2 µm.

In a metabolic labeling experiment, analysis of ^{35}S-labeled Met/Cys incorporation showed that protein biosynthesis was reduced by ∼48% in the yolk sac and by ∼45% in the embryonic tissue of *KtyII*$^{-/-}$ embryos (Fig. 3 K). Moreover, phosphorylation of the mTORC1 targets S6K and 4E-BP1 was reduced (Fig. 4 D), and eIF2-α phosphorylation was increased (Fig. 4 B). mTORC1 activity is regulated by several mechanisms, among them sequestration through 14-3-3 proteins. Previously, the skin keratin K17 was found to positively regulate protein biosynthesis and keratinocyte growth through 14-3-3–σ-mediated mTOR sequestration, suggesting a distinct role of certain keratins in wound repair (Kim et al., 2006). Although we detected sufficient 14-3-3 protein by Western blotting, the small size of embryos prevented a more detailed analysis. Given that limited glucose supply is known to severely restrict embryo growth and to increase apoptosis (Schmidt et al., 2009) and that mTORC1 is nutrient sensitive (Shaw and Cantley, 2006), we were prompted to investigate upstream regulators of mTORC1 that might depend on keratins.

Limited nutrition represses growth and protein biosynthesis, and early mouse embryos predominantly rely on glycolysis (Pantaleon and Kaye, 1998). Therefore, we analyzed the AMP kinase (AMPK), the cellular energy sensor which is phosphorylated when AMP levels are elevated (Hardie, 2007). Phosphorylated (P) AMPK inhibits the mTORC1 complex through its binding partner Raptor (Gwinn et al., 2008). Using phosphospecific antibodies, we found increases of 20% in

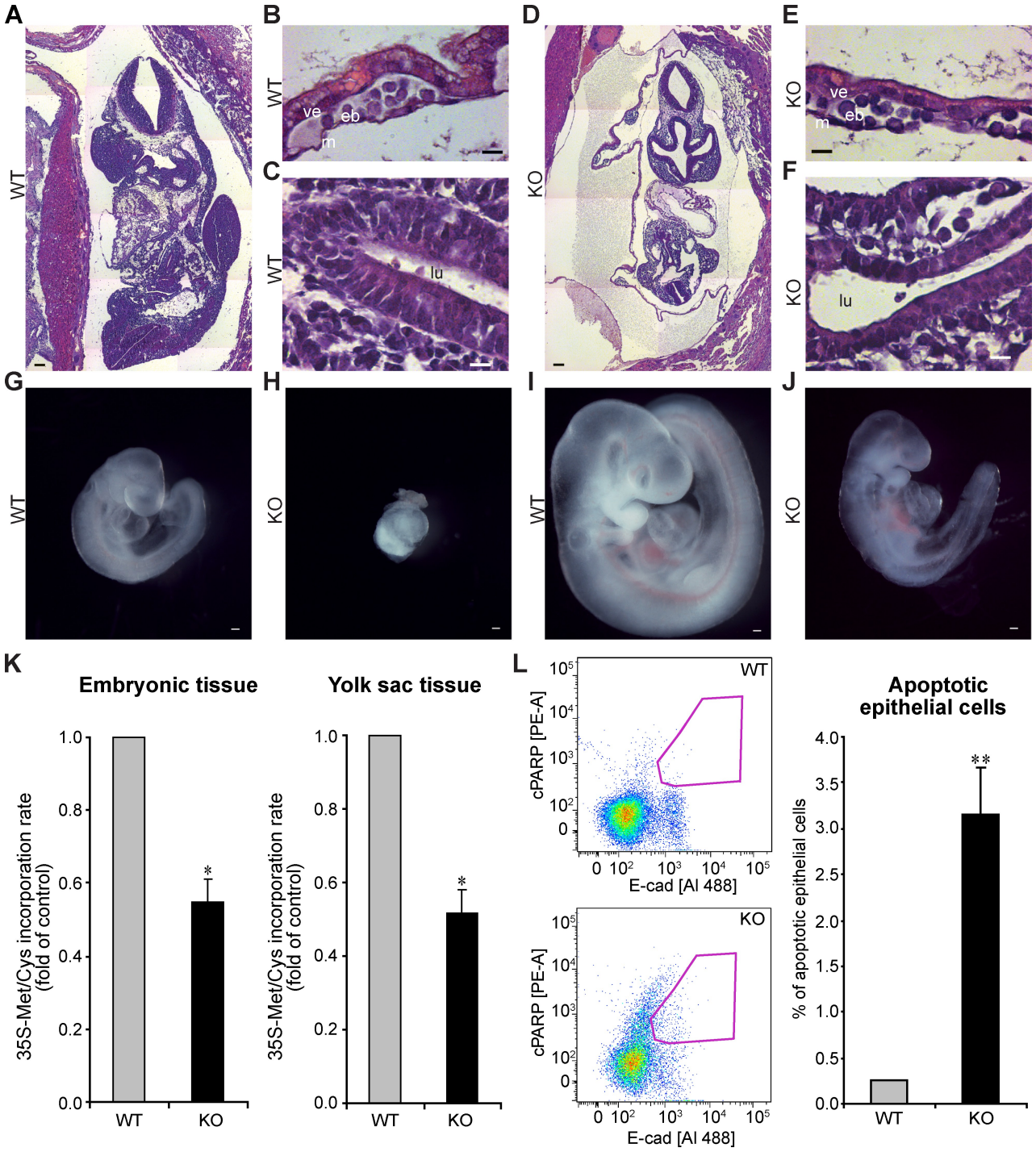

Figure 3. ***KtyII*$^{-/-}$ embryos exhibit severe growth retardation and apoptosis, resulting from reduced protein biosynthesis, but maintain tissue integrity.** (A–F) Semithin sections through WT (A–C) and mutant (D–F) embryos were stained with H&E. Note the tissue integrity in overview sections through complete E9.5 embryo in the WT (A) and the KO (D) mice. Higher magnifications of the visceral yolk sac (B and E) and embryonic intestine (C and F) from WT and KO embryos at E9.5 confirmed tissue integrity. (G–J) Whole mount photographs of WT (G and I) and mutant (H and J) embryos dissected from the yolk sac at E8.5 (G and H) and E9.5 (I and J). *KtyII*$^{-/-}$ embryos were growth retarded by ∼50%. (K) Metabolic labeling of dissected WT and *KtyII*$^{-/-}$ embryos and corresponding yolk sac tissues with ^{35}S-labeled Met/Cys. (L) FACS analysis of apoptotic cells in WT and KO embryos. Apoptosis was analyzed with cleaved poly(ADP-ribose) polymerase (cPARP) staining, and epithelial cells were detected with E-cadherin (E-cad) labeling. Subsequently, the percentage of apoptotic epithelia cells was determined to be 10-fold increased in KO compared with WT embryos. *, $P < 0.05$; **, $P < 0.005$ (two-tailed *t* test). Error bars represent SEM. eb, embryonic blood; lu, lumen; m, mesothelium; ve, visceral endoderm. Bars: (A, D, and G–J), 100 µm; (B, C, E, and F), 10 µm.

P-AMPK and 30% in P-Raptor (Fig. 4, E and F). Furthermore, we detected no change in phosphorylation of Akt, which is a positive regulator of mTOR signaling (Fig. 4 E). These findings confirmed our hypothesis that nutrient shortage, which can signal through AMPK, reduced protein synthesis in *KtyII*$^{-/-}$ embryos.

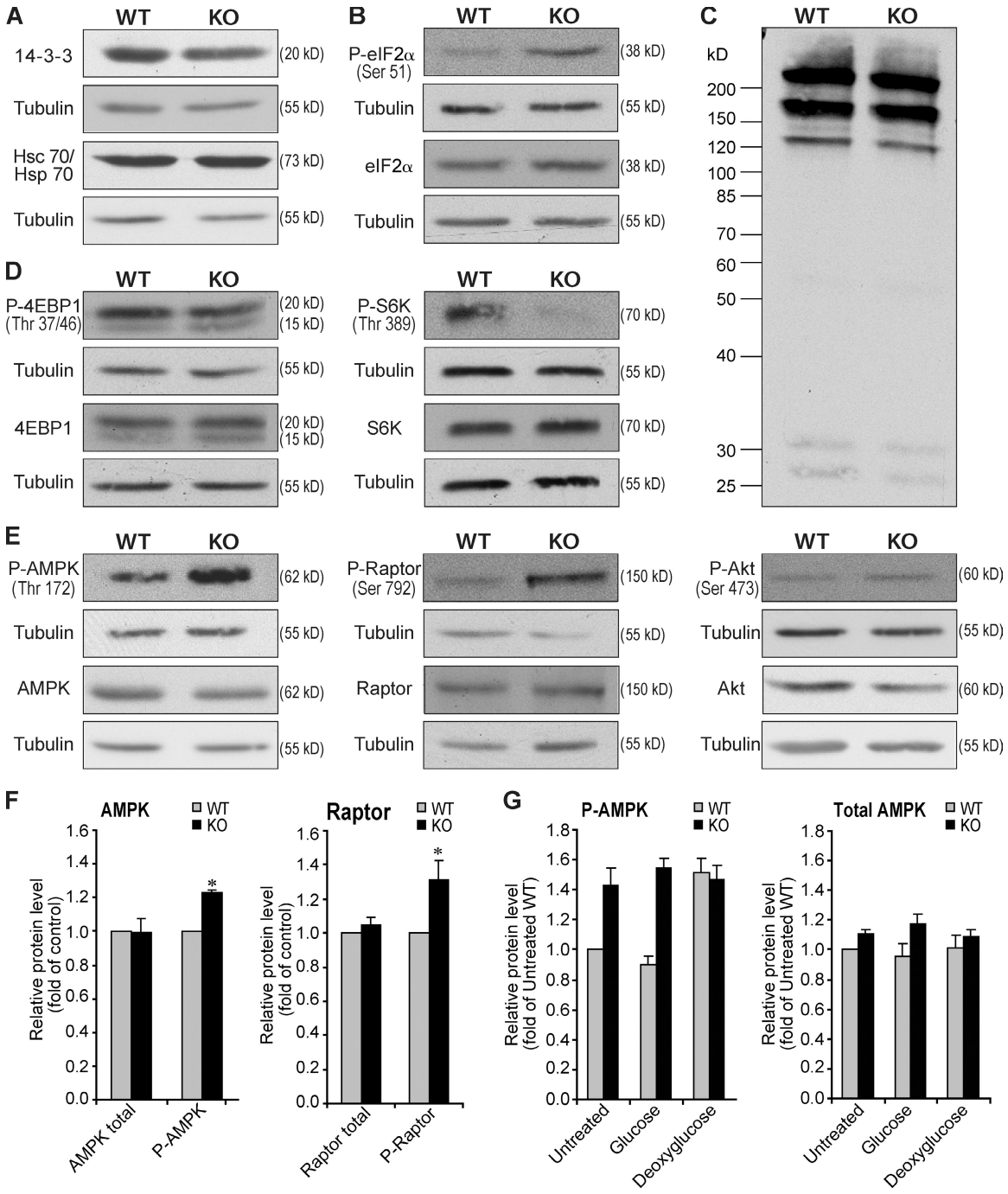

Figure 4. **Depletion of keratins activates AMPK and Raptor as the result of impaired glucose transport.** (A and C) 14-3-3, chaperones Hsc70/Hsp70 (A), and P (Thr)-MAPK/Cdk substrate levels (C) were found to be similar, comparing protein lysates of keratin WT and *KtyII*$^{-/-}$ E9.5 embryos by immunoblotting. (B and D) Detection of total and phosphorylated (P) proteins in protein lysates of keratin WT and *KtyII*$^{-/-}$ E9.5 embryos by immunoblotting of three independent pools of embryo lysates. (E and F) E9.5 lysates were analyzed by Western blotting for changes in P-AMPK and Raptor in both genotypes. Total protein and phosphoprotein levels of AMPK and Raptor were quantified by densitometry and normalized to tubulin ($n = 3$; F). (G) E9.5 embryos were incubated at 37°C for 10 min in M2^{-} medium containing 5.5 mM glucose or 5.5 mM deoxyglucose or left untreated. E9.5 lysates were Western blotted for changes in the phosphoprotein levels of AMPK in *KtyII*$^{-/-}$ and WT littermates. Total phosphoprotein levels of AMPK were quantified by densitometry and normalized to tubulin ($n = 3$). *, $P < 0.05$ (two-tailed *t* test). Error bars represent SEM.

Next, we performed a biochemical rescue experiment in which glucose was added to isolated *KtyII*$^{-/-}$ and wild-type (WT) embryos in ex vivo culture; the metabolic inhibitor deoxyglucose served as a negative control. In WT embryos, P-AMPK levels were decreased by 10% in 5 mM glucose and increased by 52% in deoxyglucose medium (Fig. 4 G). However, *KtyII*$^{-/-}$ embryos failed to respond to either treatment, indicating an unsuccessful rescue. Their P-AMPK levels were similar to those of deoxyglucose-treated WT embryos, and their total AMPK levels were unchanged (Fig. 4 G). These findings strongly suggest that keratins participate in the regulation of cellular glucose uptake.

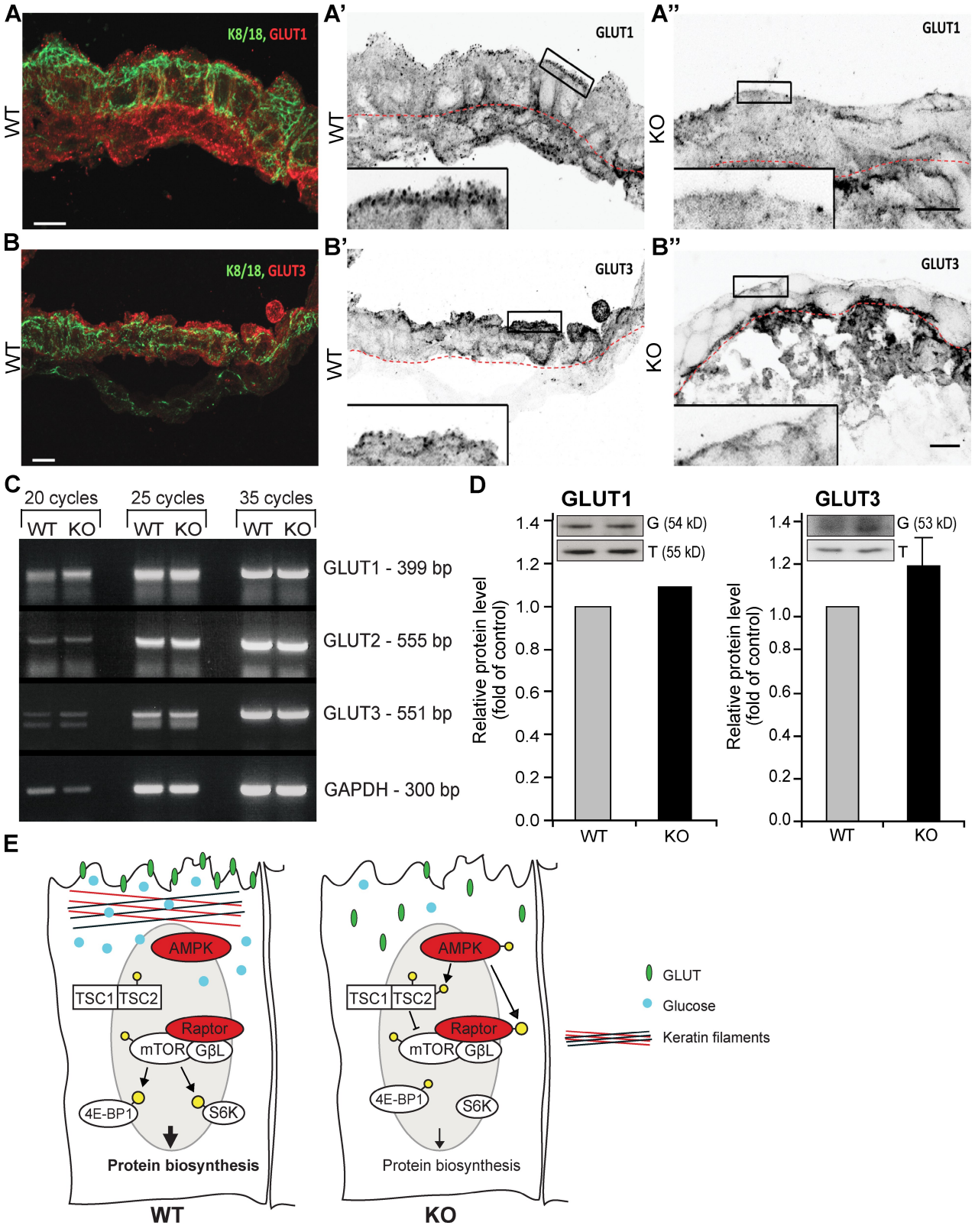

Figure 5. **Keratins regulate AMPK activity through localization of GLUT1 and -3.** (A and B) Double immunofluorescence of keratins and GLUT1 and -3 (A and B) in WT yolk sac tissue. (A′, A″, B′, and B″) Yolk sacs of E9.5 WT and *Ktyll*$^{-/-}$ embryos were analyzed for GLUT1 (A′ and A″) and -3 (B′ and B″) localization. Insets show enlargement of the region encompassing the plasma membrane. (C) mRNA expression of GLUT transporters in E9.5 WT and mutants. Glyceraldehyde 3-phosphate dehydrogenase (GAPDH) was used as a normalization control. (D) Total GLUT1 and -3 protein levels in protein lysates of E9.5 keratin WT and *Ktyll*$^{-/-}$ embryos. Error bars represent SEM. G, GLUT; T, tubulin. (E) Model for function of apical keratins in GLUT localization. Our model suggests that full activation of mTORC1 depends on the correct localization of GLUT1 and -3 by subapical keratins in the mouse embryo. Bars, 10 µm.

Glucose transport is mainly performed by energy-independent facilitative transporters of the GLUT family, which are expressed during blastocyst formation when embryos switch from pyruvate to glucose as the major energy source (Barbehenn et al., 1974). In early embryos, GLUT1 and -3 are the main transporters that regulate glucose distribution, and their KO causes severe growth retardation with increased apoptosis during embryo development (Wang et al., 2006; Ganguly et al., 2007; Schmidt et al., 2009). FACS sorting of trypsinized *KtyII*$^{-/-}$ embryos confirmed a 10-fold increase in apoptotic cells, indicating a nutrition defect (Fig. 3 L). To analyze this further, double immunofluorescence analysis with GLUT1 and -3 and K8/K18 antibodies were performed. This showed that GLUT1 and -3 were predominantly localized to the apical plasma membrane of the yolk sac. In WT yolk sacs, K8/K18 keratins were confined in the subapical region (Figs. 1 I and 5, A and B). Of note, subapical intermediate filament organization is evolutionarily conserved down to *Caenorhabditis elegans*, where it is required for gut epithelial organization (Hüsken et al., 2008). In *KtyII*$^{-/-}$ embryos, GLUT1 and -3 levels at the apical plasma membrane of the yolk sac were markedly reduced, causing redistribution of the transporters throughout endodermal cells (Fig. 5, A′, A″, B′, and B″). In line with AMPK activation, their total transcript and protein levels were unaltered (GLUT1) or slightly elevated (GLUT3; Fig. 5, C and D). Our data lead to a model in which full activation of mTORC1 depends on the correct localization of GLUT1 and -3 by subapical keratins in the mouse embryo (Fig. 5 E).

These findings reveal a novel regulatory mechanism by which keratins coordinate cell growth and protein synthesis at the level of GLUT transporters. The highly regulated expression and subcellular organization of keratins strongly suggest their involvement in growth regulation and protein targeting beyond embryo development, as demonstrated for K17 in skin wound healing and K8 in colonic epithelia (Toivola et al., 2004; Kim et al., 2006). Although the molecular mechanisms are not yet known, it is well established that the correct localization of cell adhesion proteins depends on keratins and vimentin (Godsel et al., 2005; Toivola et al., 2005; Nieminen et al., 2006). Possibly, keratins and vimentin orchestrate the local interaction of 14-3-3 proteins with their multiple binding partners during organelle transport, cell polarity, and signaling. Furthermore, our data have far-ranging implications for the analysis of other large mammalian gene families as they suggest that some of the previous single and double keratin KOs may represent gain-of-toxic-function phenotypes (Hesse et al., 2000; Tamai et al., 2000; Jaquemar et al., 2003; Magin et al., 2004). This implicates that the pathomechanisms underlying skin keratin disorders not only result from mechanical fragility but from disturbed regulation of cell growth and signaling, opening new therapeutic opportunities (Kim et al., 2006; Kerns et al., 2007; Roth et al., 2009).

Materials and methods

Targeting the 5′ end of the keratin type II cluster

The 5′ *hprt* vector clone MHPN117k13 (Adams et al., 2004) was used to target the 5′ end of the type II keratin cluster. This contained an insert of 6.0 kb spanning 101,202,450–101,208,417 bp on chromosome 15. A gap of 1.5 kb was generated with unique restriction sites, NheI and Bsp119I, to yield 2.0- and 2.4-kb arms of homology (Figs. 1 A and S1 A). NotI linkers were introduced at the cut sites to obtain a NotI restriction site. The plasmid was linearized with NotI before targeting and transfected (200 µg) into AB2.2 cells (gift from A. Bradley, Wellcome Trust Sanger Institute, Cambridge, England, UK) at 3 µF and 800 V. G418 selection was initiated 24 h after targeting at 350 µg/ml. Neomycin-resistant colonies were screened for homologous recombination; the plasmid without the gap served as a positive control. PCR primers spanned the gap region and vector backbone (Table S1). Eight clones that were PCR positive for the homologous recombination event were further confirmed by Southern blotting with a probe specific to the gap region (Table S1). Five were positive for the homologous recombination at the 5′ end of the keratin type II cluster. Clone 2 was used to target the 3′ end of the keratin type II cluster.

Targeting the 3′ end of the keratin type II cluster

The insert from the MICER 5′ *hprt* clone MHPN322c09 (Adams et al., 2004) was excised from the vector at the AscI sites flanking the insert, cloned into an empty 3′ *hprt* vector, and named MHPP322c09. This contained a 6.9-kb insert spanning 101,876,016–101,882,964 bp on chromosome 15. A gap of 1.4 kb was generated with SacI restriction sites to yield 3.0- and 2.4-kb arms of homology (Fig. 1 B and Fig. S1 A). SacI was used to linearize the plasmid to target into the aforementioned clone 2. ES cells were targeted as described in the previous section and selected in 3 µg/ml puromycin 24 h after electroporation. 8 of 96 picked clones showed homologous recombination, as determined by PCR with primers spanning the gap region and vector backbone (Table S1). These clones were confirmed by Southern blot analysis with a 487-bp probe designed within the gap region (Table S1). All PCR-positive clones were correctly recombined at the 3′ end of the keratin type II cluster, as confirmed by Southern blot analysis.

Identification of double-targeted cis ES clones by fluorescence in situ hybridization

Metaphase chromosome spreads on slides were performed as previously described (Henegariu et al., 2001). Empty 3′ and 5′ *hprt* vectors were labeled with biotin and digoxigenin, respectively, by nick translation and used for chromosomal in situ hybridization against spread chromosomes from double-targeted ES cell clones according to a standard protocol (Wrehlke et al., 1999). Red and green signals (or a yellow overlap) on a single chromosome confirmed the double targeting in cis (Fig. S1 B). One of the three double-targeted clones tested by fluorescence in situ hybridization was confirmed to have the targeted constructs in cis. This clone was subjected to Cre expression.

Cre-mediated deletion of the keratin type II cluster

The double-targeted clone in cis was transiently transfected with 200 µg of CrePac vector (Taniguchi et al., 1998) using the identical conditions described in Targeting the 5′ end of the keratin type II cluster. Selection with 1× hypoxanthine and thymine was initiated 24 h after transfection for 10 d. 96 colonies were screened for deletion of the keratin cluster with primers specific to the 3′ and 5′ *hprt* regions. This was further confirmed by Southern blot analysis with probes specific to the 3′ and 5′ *hprt* regions. Two independent clones positive for the deleted cluster were used to generate male chimeras by blastocyst injections (gift from R. Maniu, Universität Bonn, Bonn, Germany). Male chimeras were outbred to C57BL/6 WT females to generate mice heterozygous for the keratin type II deletion. Heterozygous progeny were inbred to generate *KtyII*$^{-/-}$ mice.

RT-PCR and Western blotting

Total RNA was isolated from E9.5 embryos and yolk sacs with RNeasy Micro kits (QIAGEN). Reverse transcription was performed with RevertAid First Strand cDNA Synthesis kits (Fermentas). The primers and PCR conditions have been described previously (Tonack et al., 2004; Lu et al., 2005). For vimentin cDNA synthesis, 2 µg of total RNA was reverse transcribed in a volume of 20 µl. PCR with Platinum Taq polymerase (Invitrogen) was performed in 25-µl reactions containing 0.1 µl of template cDNA, according to the manufacturer's protocol. PCR reactions were performed as follows: 35 cycles at 94°C for 30 s, 65°C for 30 s, and 72°C for 20 s. The sequences of the primer pairs are outlined in Table S1.

Western blotting was performed as follows. Total protein was extracted in SDS-PAGE sample buffer (50 mM Na phosphate, pH 6.8, 5% SDS, 40 mM DTT, 5 mM EDTA, 5 mM EGTA, and 15% glycerol). The samples were heated for 5 min at 95°C, sonicated three times for 30 s and, in between intervals, kept for 30 s at 95°C; the procedure was repeated, and

after an additional 10 min at 95°C, the insoluble material was removed by centrifugation. Total protein was determined by the protein quantification kit (Bio-Rad Laboratories), and extracts were loaded equally. Separation of total protein extracts was performed by standard procedures (8 and 10% SDS-PAGE). Proteins were electrotransferred to 0.1-µm nitrocellulose membranes (GE Healthcare) by wet blotting in Towbin buffer (25 mM Tris-HCl, pH 8.8, 192 mM glycin, 0.1% SDS, and 10% methanol). Membranes were stained with 0.5% Ponceau S. Secondary antibodies were used with Super Signal (Thermo Fisher Scientific) as a substrate (Reichelt and Magin, 2002). Antibodies and dilutions are listed in Table S2.

Histology and immunofluorescence analysis

Mouse concepti at different gestational ages were prepared. For light microscopy and immunofluorescence, tissues were snap frozen in isopentane precooled at −80°C and cryosectioned (10 µm). Immunofluorescence analysis was performed as follows: tissues were snap frozen in isopentane precooled at −80°C and stored at the same temperature. Frozen sections (8–12 µm thick) were fixed in acetone at −20°C for 10 min and dried for a few hours before further processing. All antibodies were diluted in TBS containing 1% BSA, as stated in Table S2. Primary mouse monoclonal antibodies were detected with subclass-specific secondary antibodies to minimize background. Slides were mounted in ProLong Gold antifade reagent (Invitrogen; Reichelt and Magin, 2002). Antibodies and dilutions are listed in Table S2. For routine histology, tissues were fixed overnight at 4°C in 4% formalin, sequentially incubated at 4°C overnight in 15% and 30% sucrose, embedded in paraffin, and sectioned (5 µm). Sections were placed on Superfrost Plus slides (Menzel-Gläser) and dried. After deparaffination, sections were stained with hematoxylin and eosin (H&E; Reichelt and Magin, 2002).

Immunofluorescence microscopy and data processing

The images of the H&E-stained paraffin sections were acquired using a fluorescence microscope (Axioplan 2; Carl Zeiss, Inc.) with a Plan-Neofluar 10× 0.30 NA objective and a Plan-Apochromat 63× 1.4 NA oil immersion objective at RT using a camera (AxioCam MR; Carl Zeiss, Inc.). Image analysis and processing were performed using AxioVision 4.6 (Carl Zeiss, Inc.) and Photoshop 6.0 (Adobe) software. Whole mount images were taken using a stereoscopic zoom microscope (model 1500; Nikon) with an HR Plan-Apochromat 1–3× zoom objective at RT using a camera (DS-U2/L2; Nikon). Image analysis and processing were performed with Photoshop software. Immunofluorescent samples were analyzed with a fluorescence laser-scanning confocal microscope (LSM 710; Carl Zeiss, Inc.). For immunofluorescence microscopy and data processing, image stacks were collected with confocal microscope (TCS SP5; Leica) or a laser-scanning microscope (LSM 710) with a Plan-Apochromat 63× 1.4 NA oil immersion objective at RT, and projection views of stacks were produced with the aid of Amira software (Visage Imaging). LUT (lookup table; brightness and gamma) was adjusted using Photoshop. In some instances, single focal planes are shown.

Flow cytometry

E9.5 embryos were trypsinized, and single-cell suspensions were fixed in 2% PFA/PBS for 10 min at 4°C, washed with PBS, and permeabilized with 0.25% Triton X-100/PBS for 5 min at 4°C. The cells were washed and then stained for 30 min at 4°C with E-cadherin (Invitrogen) in 0.5% BSA/TBS and, after washing, were labeled with goat anti–rat Alexa Fluor 488 (Dianova) for 15 min at 4°C. Cells were washed again and stained for 30 min at RT with cleaved poly(ADP-ribose) polymerase–phycoerythrin (BD) in 0.5% BSA/TBS. Cells were sorted on a flow fluorocytometer (FACSCanto II or LSRII; BD), and data were analyzed using FlowJo software (Tree Star, Inc.).

Antibodies

We used antibodies against biotinylated antiavidin (Vector Laboratories), antidigoxigenin (Boehringer Ingelheim), K8/K18 (Progen), K19 (Troma-3; American Type Culture Collection), desmoplakin (gift from D. Garrod, University of Manchester, Manchester, England, UK), vimentin (T.M. Magin laboratory), ZO-1 (Zytomed Systems GmbH), occludin (Invitrogen), E-cadherin (Invitrogen), ninein (gift from J.B. Rattner, University of Calgary, Calgary, Alberta, Canada), 4E-BP1, P–4E-BP1 (Thr37/46), p70 S6K, P–p70 S6K (Thr389), eIF2-α, P–eIF2-α (Ser51), AMPK, P–AMPK-α (Thr172), Raptor, P-Raptor (Ser792), Akt, P-Akt (Ser473), P (Thr)-MAPK/Cdk substrates (all from Cell Signaling Technology), GLUT1 (Millipore), GLUT3 (Alpha Diagnostic International, Inc.), Hsc70/Hsp70 (Stressgen), 14-3-3–β (Santa Cruz Biotechnology, Inc.), and secondary antibodies (Dianova). Dilutions are listed in Table S2.

Metabolic labeling

E9.5 embryos and yolk sacs were dissected from the uterus, and the head was retained for genotyping. Embryos and yolk sac were incubated separately in Met-free Dulbecco's modified Eagle's medium (Invitrogen) containing 25 mM Hepes buffer, 10% dialyzed fetal calf serum, 1% nonessential amino acids, 1× Na pyruvate, and 1% Glutamax (all Invitrogen) at 37°C for 15 min to remove endogenous Met. The medium was discarded, and tissues were labeled with 100 µl of ^{35}S-labeled Met/Cys (1,000 Ci/mmol; 0.1 mCi/ml) in Met-free Dulbecco's modified Eagle's medium for 1 h at 37°C. The medium was aspirated, and tissues were washed in ice-cold PBS. Proteins were precipitated with 10% trichloroacetic acid, and incorporated radioactivity was measured by liquid scintillation. The rate of ^{35}S-labeled Met/Cys incorporation per minute per milligram of protein was calculated using the Bradford reagent (Bradford, 1976).

Glucose assay

E9.5 embryos and yolk sacs were dissected from the uterus. Embryos and yolk sac together were incubated in M2$^-$ medium (94.59 mM NaCl, 4.78 mM KCl, 1.19 mM KH_2PO_4, 1.19 $MgSO_4$, 1.71 mM $CaCl_2$, 4.0 mM $NaHCO_3$, 21 mM Hepes, and 4 g/liter albumin bovine fraction V; all from Sigma-Aldrich) without glucose or its metabolites, with 5.5 mM glucose (Sigma-Aldrich), or with 5.5 mM deoxyglucose (Sigma-Aldrich) for 10 min at 37°C. Subsequently, embryos were lysed in boiling Laemmli buffer and analyzed by Western blotting for total and P-AMPK levels.

Online supplemental material

Fig. S1 shows additional characterizations of the genetic engineering at the keratin type II gene locus. Fig. S2 demonstrates that the deletion of keratins does not induce vimentin. Tables S1 and S2 provide the details of the primers and the antibodies, respectively, used in this study. Online supplemental material is available at http://www.jcb.org/cgi/content/full/jcb.200906094/DC1.

We thank Prof. A. Bradley for providing the AB2.2 ES cell line, snlp feeder cell line, and MICER clones for targeting and Mrs. R. Maniu for the blastocyst injections. We gratefully thank Prof. J.B. Rattner for his gift of ninein antiserum and E. Endl, A. Dolf, and P. Wurst from the Flow Cytometry Core Facility at the Institute for Molecular Medicine and Experimental Immunology, University of Bonn. We thank our former colleague Dr. M. Hesse for stimulating ideas and input in the experimental design. We are grateful to our colleagues M. Hatzfeld and M. Hoch for critical input. Also, we thank colleagues who provided antibodies.

This project was funded by Deutsche Forschungsgemeinschaft (German Research Council MA 1316/7) grant SFB832, Bonfor (Cytoskeletal Research Group), and the Bonner Forum Biomedizin.

Submitted: 15 June 2009
Accepted: 2 September 2009

References

Adams, D.J., P.J. Biggs, T. Cox, R. Davies, L. van der Weyden, J. Jonkers, J. Smith, B. Plumb, R. Taylor, I. Nishijima, et al. 2004. Mutagenic insertion and chromosome engineering resource (MICER). *Nat. Genet.* 36:867–871. doi:10.1038/ng1388

Ameen, N.A., Y. Figueroa, and P.J. Salas. 2001. Anomalous apical plasma membrane phenotype in CK8-deficient mice indicates a novel role for intermediate filaments in the polarization of simple epithelia. *J. Cell Sci.* 114:563–575.

Barbehenn, E.K., R.G. Wales, and O.H. Lowry. 1974. The explanation for the blockade of glycolysis in early mouse embryos. *Proc. Natl. Acad. Sci. USA*. 71:1056–1060. doi:10.1073/pnas.71.4.1056

Baribault, H., J. Price, K. Miyai, and R.G. Oshima. 1993. Mid-gestational lethality in mice lacking keratin 8. *Genes Dev.* 7:1191–1202. doi:10.1101/gad.7.7a.1191

Betz, R.C., L. Planko, S. Eigelshoven, S. Hanneken, S.M. Pasternack, H. Bussow, K. Van Den Bogaert, J. Wenzel, M. Braun-Falco, A. Rutten, et al. 2006. Loss-of-function mutations in the keratin 5 gene lead to Dowling-Degos disease. *Am. J. Hum. Genet.* 78:510–519. doi:10.1086/500850

Bradford, M.M. 1976. A rapid and sensitive method for the quantitation of microgram quantities of protein utilizing the principle of protein-dye binding. *Anal. Biochem.* 72:248–254. doi:10.1016/0003-2697(76)90527-3

Fuchs, E., and D.W. Cleveland. 1998. A structural scaffolding of intermediate filaments in health and disease. *Science*. 279:514–519. doi:10.1126/science.279.5350.514

Ganguly, A., R.A. McKnight, S. Raychaudhuri, B.C. Shin, Z. Ma, K. Moley, and S.U. Devaskar. 2007. Glucose transporter isoform-3 mutations cause early pregnancy loss and fetal growth restriction. *Am. J. Physiol. Endocrinol. Metab.* 292:E1241–E1255. doi:10.1152/ajpendo.00344.2006

Godsel, L.M., S.N. Hsieh, E.V. Amargo, A.E. Bass, L.T. Pascoe-McGillicuddy, A.C. Huen, M.E. Thorne, C.A. Gaudry, J.K. Park, K. Myung, et al. 2005. Desmoplakin assembly dynamics in four dimensions: multiple phases differentially regulated by intermediate filaments and actin. *J. Cell Biol.* 171:1045–1059. doi:10.1083/jcb.200510038

Gwinn, D.M., D.B. Shackelford, D.F. Egan, M.M. Mihaylova, A. Mery, D.S. Vasquez, B.E. Turk, and R.J. Shaw. 2008. AMPK phosphorylation of raptor mediates a metabolic checkpoint. *Mol. Cell*. 30:214–226. doi:10.1016/j.molcel.2008.03.003

Hardie, D.G. 2007. AMP-activated/SNF1 protein kinases: conserved guardians of cellular energy. *Nat. Rev. Mol. Cell Biol.* 8:774–785. doi:10.1038/nrm2249

Henegariu, O., N.A. Heerema, L. Lowe Wright, P. Bray-Ward, D.C. Ward, and G.H. Vance. 2001. Improvements in cytogenetic slide preparation: controlled chromosome spreading, chemical aging and gradual denaturing. *Cytometry*. 43:101–109. doi:10.1002/1097-0320(20010201)43:2<101::AID-CYTO1024>3.0.CO;2-8

Hesse, M., T. Franz, Y. Tamai, M.M. Taketo, and T.M. Magin. 2000. Targeted deletion of keratins 18 and 19 leads to trophoblast fragility and early embryonic lethality. *EMBO J.* 19:5060–5070. doi:10.1093/emboj/19.19.5060

Hesse, M., T.M. Magin, and K. Weber. 2001. Genes for intermediate filament proteins and the draft sequence of the human genome: novel keratin genes and a surprisingly high number of pseudogenes related to keratin genes 8 and 18. *J. Cell Sci.* 114:2569–2575.

Hesse, M., A. Zimek, K. Weber, and T.M. Magin. 2004. Comprehensive analysis of keratin gene clusters in humans and rodents. *Eur. J. Cell Biol.* 83:19–26. doi:10.1078/0171-9335-00354

Hüsken, K., T. Wiesenfahrt, C. Abraham, R. Windoffer, O. Bossinger, and R.E. Leube. 2008. Maintenance of the intestinal tube in *Caenorhabditis elegans*: the role of the intermediate filament protein IFC-2. *Differentiation*. 76:881–896. doi:10.1111/j.1432-0436.2008.00264.x

Jackson, B.W., C. Grund, E. Schmid, K. Bürki, W.W. Franke, and K. Illmensee. 1980. Formation of cytoskeletal elements during mouse embryogenesis. Intermediate filaments of the cytokeratin type and desmosomes in preimplantation embryos. *Differentiation*. 17:161–179. doi:10.1111/j.1432-0436.1980.tb01093.x

Jaquemar, D., S. Kupriyanov, M. Wankell, J. Avis, K. Benirschke, H. Baribault, and R.G. Oshima. 2003. Keratin 8 protection of placental barrier function. *J. Cell Biol.* 161:749–756. doi:10.1083/jcb.200210004

Kerns, M.L., D. DePianto, A.T. Dinkova-Kostova, P. Talalay, and P.A. Coulombe. 2007. Reprogramming of keratin biosynthesis by sulforaphane restores skin integrity in epidermolysis bullosa simplex. *Proc. Natl. Acad. Sci. USA*. 104:14460–14465. doi:10.1073/pnas.0706486104

Kim, S., and P.A. Coulombe. 2007. Intermediate filament scaffolds fulfill mechanical, organizational, and signaling functions in the cytoplasm. *Genes Dev.* 21:1581–1597. doi:10.1101/gad.1552107

Kim, S., P. Wong, and P.A. Coulombe. 2006. A keratin cytoskeletal protein regulates protein synthesis and epithelial cell growth. *Nature*. 441:362–365. doi:10.1038/nature04659

Lechler, T., and E. Fuchs. 2005. Asymmetric cell divisions promote stratification and differentiation of mammalian skin. *Nature*. 437:275–280. doi:10.1038/nature03922

Liao, J., D. Price, and M.B. Omary. 1997. Association of glucose-regulated protein (grp78) with human keratin 8. *FEBS Lett.* 417:316–320. doi:10.1016/S0014-5793(97)01315-X

Lu, H., M. Hesse, B. Peters, and T.M. Magin. 2005. Type II keratins precede type I keratins during early embryonic development. *Eur. J. Cell Biol.* 84:709–718. doi:10.1016/j.ejcb.2005.04.001

Magin, T.M., R. Schröder, S. Leitgeb, F. Wanninger, K. Zatloukal, C. Grund, and D.W. Melton. 1998. Lessons from keratin 18 knockout mice: formation of novel keratin filaments, secondary loss of keratin 7 and accumulation of liver-specific keratin 8-positive aggregates. *J. Cell Biol.* 140:1441–1451. doi:10.1083/jcb.140.6.1441

Magin, T.M., J. Reichelt, and M. Hatzfeld. 2004. Emerging functions: diseases and animal models reshape our view of the cytoskeleton. *Exp. Cell Res.* 301:91–102. doi:10.1016/j.yexcr.2004.08.018

Magin, T.M., P. Vijayaraj, and R.E. Leube. 2007. Structural and regulatory functions of keratins. *Exp. Cell Res.* 313:2021–2032. doi:10.1016/j.yexcr.2007.03.005

Nieminen, M., T. Henttinen, M. Merinen, F. Marttila-Ichihara, J.E. Eriksson, and S. Jalkanen. 2006. Vimentin function in lymphocyte adhesion and transcellular migration. *Nat. Cell Biol.* 8:156–162. doi:10.1038/ncb1355

Pantaleon, M., and P.L. Kaye. 1998. Glucose transporters in preimplantation development. *Rev. Reprod.* 3:77–81. doi:10.1530/ror.0.0030077

Ramírez-Solis, R., P. Liu, and A. Bradley. 1995. Chromosome engineering in mice. *Nature*. 378:720–724. doi:10.1038/378720a0

Reichelt, J., and T.M. Magin. 2002. Hyperproliferation, induction of c-Myc and 14-3-3sigma, but no cell fragility in keratin-10-null mice. *J. Cell Sci.* 115:2639–2650.

Roth, W., U. Reuter, C. Wohlenberg, L. Bruckner-Tuderman, and T.M. Magin. 2009. Cytokines as genetic modifiers in K5-/- mice and in human epidermolysis bullosa simplex. *Hum. Mutat.* 30:832–841. doi:10.1002/humu.20981

Schmidt, S., A. Hommel, V. Gawlik, R. Augustin, N. Junicke, S. Florian, M. Richter, D.J. Walther, D. Montag, H.G. Joost, and A. Schürmann. 2009. Essential role of glucose transporter GLUT3 for post-implantation embryonic development. *J. Endocrinol.* 200:23–33. doi:10.1677/JOE-08-0262

Schweizer, J., P.E. Bowden, P.A. Coulombe, L. Langbein, E.B. Lane, T.M. Magin, L. Maltais, M.B. Omary, D.A. Parry, M.A. Rogers, and M.W. Wright. 2006. New consensus nomenclature for mammalian keratins. *J. Cell Biol.* 174:169–174. doi:10.1083/jcb.200603161

Shaw, R.J., and L.C. Cantley. 2006. Ras, PI(3)K and mTOR signalling controls tumour cell growth. *Nature*. 441:424–430. doi:10.1038/nature04869

Tamai, Y., T. Ishikawa, M.R. Bösl, M. Mori, M. Nozaki, H. Baribault, R.G. Oshima, and M.M. Taketo. 2000. Cytokeratins 8 and 19 in the mouse placental development. *J. Cell Biol.* 151:563–572. doi:10.1083/jcb.151.3.563

Taniguchi, M., M. Sanbo, S. Watanabe, I. Naruse, M. Mishina, and T. Yagi. 1998. Efficient production of Cre-mediated site-directed recombinants through the utilization of the puromycin resistance gene, pac: a transient gene-integration marker for ES cells. *Nucleic Acids Res.* 26:679–680. doi:10.1093/nar/26.2.679

Thiery, J.P. 2002. Epithelial-mesenchymal transitions in tumour progression. *Nat. Rev. Cancer*. 2:442–454. doi:10.1038/nrc822

Toivola, D.M., S. Krishnan, H.J. Binder, S.K. Singh, and M.B. Omary. 2004. Keratins modulate colonocyte electrolyte transport via protein mistargeting. *J. Cell Biol.* 164:911–921. doi:10.1083/jcb.200308103

Toivola, D.M., G.Z. Tao, A. Habtezion, J. Liao, and M.B. Omary. 2005. Cellular integrity plus: organelle-related and protein-targeting functions of intermediate filaments. *Trends Cell Biol.* 15:608–617. doi:10.1016/j.tcb.2005.09.004

Tonack, S., B. Fischer, and A. Navarrete Santos. 2004. Expression of the insulin-responsive glucose transporter isoform 4 in blastocysts of C57/BL6 mice. *Anat. Embryol. (Berl.)*. 208:225–230.

Wang, D., J.M. Pascual, H. Yang, K. Engelstad, X. Mao, J. Cheng, J. Yoo, J.L. Noebels, and D.C. De Vivo. 2006. A mouse model for Glut-1 haploinsufficiency. *Hum. Mol. Genet.* 15:1169–1179. doi:10.1093/hmg/ddl032

Wrehlke, C., W.R. Wiedemeyer, H.P. Schmitt-Wrede, A. Mincheva, P. Lichter, and F. Wunderlich. 1999. Genomic organization of mouse gene zfp162. *DNA Cell Biol.* 18:419–428. doi:10.1089/104454999315303

Wullschleger, S., R. Loewith, and M.N. Hall. 2006. TOR signaling in growth and metabolism. *Cell*. 124:471–484. doi:10.1016/j.cell.2006.01.016

Yang, J., and R.A. Weinberg. 2008. Epithelial-mesenchymal transition: at the crossroads of development and tumor metastasis. *Dev. Cell*. 14:818–829. doi:10.1016/j.devcel.2008.05.009